Published in final edited form as:
Neuroscience. 2014 September 26; 277: 552–567. doi:10.1016/j.neuroscience.2014.07.029.

Strain-Dependent Brain Defects in Mouse Models of Primary Ciliary Dyskinesia with Mutations in *Pcdp1* and *Spef2*

Rozzy Finn[a], **Claire C. Evans**[b], and **Lance Lee**[a,c]

Rozzy Finn: Rozzy.Finn@sanfordhealth.org; Claire C. Evans: Claire.Evans@sanfordhealth.org

[a]Sanford Children's Health Research Center, Sanford Research, 2301 E. 60th St. N., Sioux Falls, SD, USA 57104

[b]Cancer Biology Research Center, Sanford Research, 2301 E. 60th St. N., Sioux Falls, SD, USA 57104

[c]Department of Pediatrics, Sanford School of Medicine of the University of South Dakota, Sioux Falls, SD 57105

Abstract

Hydrocephalus is caused by the accumulation of cerebrospinal fluid in the cerebral ventricular system which results in an enlargement of the cranium due to increased intraventricular pressure. The increase in pressure within the brain typically results in sloughing of ciliated ependymal cells, loss of cortical grey matter, and increased gliosis. Congenital hydrocephalus is associated with several syndromes including primary ciliary dyskinesia (PCD), a rare, genetically heterogeneous, pediatric syndrome that results from defects in motile cilia and flagella. We have examined the morphological and physiological defects in the brains of two mouse models of PCD, *nm1054* and *bgh*, which have mutations in *Pcdp1* (also known as *Cfap221*) and *Spef2*, respectively. Histopathological and immunohistochemical analyses of mice with these mutations on the C57BL/6J and 129S6/SvEvTac genetic backgrounds demonstrate strain-dependent morphological brain damage. Alterations in astrocytosis, microglial activation, myelination, and the neuronal population were identified and are generally more severe on the C57BL/6J background. Analysis of ependymal ciliary clearance *ex vivo* and cerebrospinal fluid flow *in vivo* demonstrate a physiological defect in *nm1054* and *bgh* mice on both genetic backgrounds, indicating that abnormal cilia-driven flow is not the sole determinant of the severity of hydrocephalus in these models. These results suggest that genetic modifiers play an important role in susceptibility to severe PCD-associated hydrocephalus.

Keywords

Cilia; Hydrocephalus; Primary Ciliary Dyskinesia; Pcdp1; Cfap221; Spef2

Corresponding Author: Lance Lee, PhD, Sanford Children's Health Research Center, Sanford Research, 2301 E. 60th St. N., Sioux Falls, SD, USA 57104, Telephone: 605-312-6410, FAX: 605-312-6071, Lance.Lee@sanfordhealth.org.

1. Introduction

Congenital hydrocephalus is a birth defect occurring with a frequency of approximately 1-3 in 1000 newborn children that is caused by an accumulation of cerebrospinal fluid (CSF) in the cerebral ventricular system (Chiafery, 2006; Del Bigio, 2001; Del Bigio, 2004; Mataro et al., 2001; Perez-Figares et al., 2001; Rekate, 1997; Zhang et al., 2006). This excess CSF results in an enlargement of the cranium due to an increase in intraventricular pressure. Patients suffering from congenital hydrocephalus commonly experience vomiting, sleepiness, and seizures. If left untreated, individuals are frequently afflicted with headaches, visual deficits, ataxia, cognitive dysfunction, and premature death. Currently, the only available treatments for hydrocephalus involve the surgical insertion of a shunt to drain CSF from the ventricles or an alternative surgical procedure called endoscopic third ventriculostomy, both of which can result in complications and necessitate follow-up medical care (Browd et al., 2006a; Browd et al., 2006b; Chiafery, 2006; Drake, 2008; Hanigan et al., 1991; Kang and Lee, 1999; Khan et al., 2007; Mataro et al., 2001; Rekate, 1997).

Hydrocephalus may be either communicating or obstructive (Chiafery, 2006; Del Bigio, 2001; Del Bigio, 2004; Mataro et al., 2001; Perez-Figares et al., 2001; Rekate, 1997; Zhang et al., 2006). In communicating hydrocephalus, CSF flow is inhibited, often due to defects in CSF production, flow, or reabsorption. Obstructive hydrocephalus results from blockage of flow within the ventricular system by obstruction or constriction and is classified based on point of obstruction (Rekate, 2011). In both types of hydrocephalus, CSF accumulation leads to excessive intraventricular pressure, typically resulting in the sloughing of the ciliated ependymal cells, loss of cortical gray matter, and gliosis (Del Bigio, 2001; Del Bigio, 2004; Dominguez-Pinos et al., 2005; Mataro et al., 2001). In humans, non-syndromic congenital hydrocephalus has been linked to three associated genes: *L1 cell adhesion molecule* (*L1CAM*) on the X chromosome (Jouet et al., 1993), the Wnt pathway inhibitor *CCDC88C* (Ekici et al., 2010), and *MPDZ*, which encodes a multiple PDZ domain protein associated with tight junctions (Al-Dosari et al., 2013). Mouse models have identified myriad additional genes associated with congenital hydrocephalus, including transcription factors, cadherins, and cytokine signaling suppressors (Lee, 2013). Congenital hydrocephalus is also associated with a variety of genetic syndromes, including primary ciliary dyskinesia (PCD) (Lee, 2013). A more complete understanding of genetic and molecular causes of hydrocephalus is required to improve diagnosis and treatment.

PCD, a genetically heterogeneous, pediatric syndrome, affects approximately 1 in 16,000 newborns (Afzelius, 2004; Chodhari et al., 2004; Horani et al., 2014; Ibanez-Tallon et al., 2003; Knowles et al., 2013; Lee, 2011; Leigh et al., 2009). Affected patients are commonly afflicted with chronic rhinosinusitis, otitis media, and male infertility, with situs inversus, hydrocephalus, and female infertility also occurring in some patients. PCD results from defects in the structure and function of motile cilia, microtubule-based organelles that play a role in the motility of fluids and cells within the respiratory system, cerebral ventricles, and reproductive system. Motile cilia function through a coordinated beating motion driven by the planar cell polarity signaling pathway (Chodhari et al., 2004; Wallingford, 2010). Within

the cilium, nine pairs of microtubules surround an additional central pair, giving rise to a 9+2 ultrastructure (Afzelius, 2004; Chodhari et al., 2004; Lee, 2011; Satir and Christensen, 2007). Cilia located on the embryonic node lack a central pair and are responsible for left-right patterning. Motile cilia are structurally related to flagella, which are present on spermatozoa and single celled organisms such as *Chlamydomonas reinhardtii* and are required for cell motility. The immotile primary cilia found on other cell types, which have a 9+0 microtubule structure and a mechanosensory function, are unaffected in PCD patients (Berbari et al., 2009; Guemez-Gamboa et al., 2014).

Hydrocephalus has been observed in numerous mouse models of PCD (Lee, 2013). The *nm1054* and *big giant head* (*bgh*) models were previously characterized on both the C57BL/6J (B6) and 129S6/SvEvTac (129) backgrounds (Lee et al., 2008; Sironen et al., 2011). The PCD in both models is characterized by hydrocephalus, male infertility, and respiratory abnormalities that result from cilia with a reduced beat frequency (Lee et al., 2008; McKenzie et al., 2013; Sironen et al., 2011). However, severe gross hydrocephalus was only observed on the B6 background, suggesting the presence of genetic modifiers of the hydrocephalus. The *nm1054* mouse possesses a 400 kb deletion on chromosome 1 that results in the disruption of six different genes (Lee et al., 2008; Lee et al., 2007; Ohgami et al., 2005a; Ohgami et al., 2005b). Transgenic rescue demonstrated that deletion of the *primary ciliary dyskinesia protein 1 (Pcdp1)* gene, also known as *ciliary and flagellar associated protein 221 (Cfap221)*, induces the reported PCD phenotype (Lee et al., 2008), and studies in *C. reinhardtii* have shown that Pcdp1 is a central pair protein that regulates ciliary motility via interactions with Ca^{2+}-Calmodulin (DiPetrillo and Smith, 2010). The *bgh* PCD results from a mutation in the *Sperm flagellar protein 2* (*Spef2*) gene (Lambe et al., 2009; Sironen et al., 2011). Spef2 is thought to be involved in intraflagellar transport and is the likely homolog of the *C. reinhardtii* protein Central pair complex 1 (Cpc1) (Sironen et al., 2010; Sironen et al., 2011; Sironen et al., 2006; Zhang and Mitchell, 2004).

To further understand the hydrocephalus in the *nm1054* and *bgh* models, we have extensively analyzed the morphological and physiological defects in mutant brains on both the B6 and the 129 backgrounds. Structural damage and disruption of numerous cell types correlate with the severity of hydrocephalus and are generally more severe on the B6 background. Functional disruption of CSF flow and a defect in ependymal ciliary function, however, were observed in both PCD mutants on both genetic backgrounds, suggesting that abnormal cilia-driven flow is not the sole determinant of severe hydrocephalus in these models.

2. Materials and Methods

2.1. Animals

The *nm1054* and *bgh* mouse lines were maintained on the C57BL/6J (B6) and 129S6/SvEvTac (129) backgrounds. Mice were analyzed at three weeks of age. The *nm1054* mice on the B6 background rarely live to weaning age due to severe hydrocephalus and anemia (Lee et al., 2008; Ohgami et al., 2005a). To enable the analysis of three-week-old mice, we analyzed animals expressing the RPCI-22 bacterial artificial chromosome 11D19, which contains the *Steap3* gene, to rescue the anemia (Ohgami et al., 2005b). All experiments were

carried out in accordance with the Animal Welfare Act, NIH policies, and the Sanford Research Institutional Animal Care and Use Committee.

2.2. Histology and Immunohistochemistry

Heads from *nm1054*, *bgh* and wild type (WT) animals on both backgrounds were immersion fixed in Bouin's fixative until bones had sufficiently decalcified. To preserve the neural architecture to the fullest extent, a 5 mm coronal slice was cut through the whole head and embedded in paraffin using a 300 ASP tissue processor (Leica). Coronal sections were then cut at a thickness of 5 μm and stained with hematoxylin and eosin (H&E) using a Tissue-Tek automated H&E stainer (Sakura). Slides were viewed using a 90i upright microscope (Nikon) and imaged with a Digital Sight DS-2Mv camera (Nikon). Three to six mice were used for all histological analyses.

The BenchMark® XT automated slide staining system (Ventana Medical Systems, Inc.) was used for immunohistochemical analysis of the coronal sections. Cilia were labeled using anti-acetylated tubulin (Sigma-Aldrich, T7451) (McKenzie et al., 2013) at a 1:6000 dilution. Glia were labeled using anti-GFAP (Dako, Z0334) (Thelen et al., 2012) at a 1:500 dilution, anti-Iba1 (BioCare Medical, CP290) (Woodruff et al., 2008) at a 1:100 dilution, and anti-CD68 (AbD Serotec, MCA1957) (Thelen et al., 2012) at a 1:25 dilution. White matter was visualized using anti-MBP (Millipore, NE1018) (Markakis et al., 2009; Steffenhagen et al., 2012) at a 1:1000 dilution. Cortical neurons were imaged using anti-MAP2 (Millipore, MAB3418) (Falcao et al., 2013; Srivastava et al., 2012) at a 1:500 dilution. Biotin-SP-conjugated AffiniPure Goat Anti-Rabbit IgG, Biotin-SP-conjugated AffiniPure Donkey Anti-Mouse IgG and Biotin-SP-conjugated AffiniPure Goat Anti-Rat IgG (Jackson ImmunoResearch) were diluted 1:1000 and used as secondary antibodies. The Ventana iView DAB detection kit was used for detection, and all slides were counterstained with hematoxylin. Slides were viewed using a 90i upright microscope (Nikon) and imaged with a Digital Sight DS-2Mv camera (Nikon). Three to six mice were used for all immunohistochemical analyses.

2.3. Ependymal Ciliary Clearance Assay

Brains from *nm1054*, *bgh*, and WT mice on both backgrounds were dissected in phosphate buffered saline (PBS) to expose the wall of the lateral ventricle as previously described (Mirzadeh et al., 2010). After dissection, the exposed wall was moved to a sylguard-coated glass dish (Dow Corning, Pyrex) containing fresh PBS and immobilized with pins. A small amount (< 0.5 μl) of India ink diluted to 50% in PBS with 10% glycerol was deposited onto the ependymal surface using a Wiretrol pipet. Ink movement was recorded using an SMZ1000 stereomicroscope and DS-Fi1 camera and analyzed with NIS Elements software (Nikon). For each animal, the distance that ependymal cilia moved the ink stream within two seconds was measured using the NIS Elements software, and this measurement was used to calculate the flow rate. Microsoft Excel was used to perform a two tailed t-test to determine statistical significance. n=11 WT B6, 6 WT 129, 3 *nm1054* B6, 6 *nm1054* 129, 6 *bgh* B6, and 6 *bgh* 129 animals.

2.4. CSF Flow Analysis

WT, *nm1054*, and *bgh* animals on both backgrounds were intraperitoneally injected with 15 μl/g Avertin (2% 2,2,2-tribromoethanol; Sigma). When no longer responsive, mice were immobilized in a stereotaxic device (Stoeling). The right lateral ventricle was injected with 1 μl India ink using the following coordinates: 1.5 mm anterior to bregma, 1 mm lateral of the midline, and 3 mm deep. As mutant animals ranged in size depending upon genetic background, coordinates for injecting smaller mutant animals (*nm1054* and *bgh* on the B6 background) were amended to 1 mm anterior to bregma and 0.75 mm lateral, with injection depth kept constant. One minute after ink injection, animals were sacrificed by cervical dislocation, and heads were immersion fixed in Bouin's fixative. Coronal sections were generated as described above and stained with cresyl violet. n=7 WT B6, 7 WT 129, 5 *nm1054* B6, 7 *nm1054* 129, 7 *bgh* B6, and 5 *bgh* 129.

3. Results

3.1. *nm1054* and *bgh* mutant brains have morphological damage with strain-dependent severity

Histological examination of brains from *nm1054* and *bgh* mice demonstrates ventricular dilatation in addition to notable damage to the white matter (Fig. 1 A-F). For each mutant, the severity of the neurological damage is dependent upon the genetic background on which it is maintained. The lateral ventricle in WT mice is a narrow space (Fig. 1 A, D). In contrast, *nm1054* animals maintained on the B6 background demonstrate a severe pathology with dramatic dilatation of the lateral ventricles (Fig. 1 B). Separation of the ependyma from the damaged white matter is also visible (Fig. 1 B). The *bgh* brains on the B6 background have a similarly severe phenotype (Fig. 1 C) as was previously demonstrated (Sironen et al., 2011). The ventricular dilatation in both mutants is likely due to the accumulation of CSF in the lateral ventricles, and resulting intraventricular pressure is likely responsible for the ependymal sloughing and white matter damage as typically seen in hydrocephalic brains (Del Bigio, 2001; Del Bigio, 2004; Dominguez-Pinos et al., 2005; Mataro et al., 2001). For both mutants, the observed damage is less severe on the 129 background (Fig. 1 E, F). The *nm1054* mutants have only mild ventricular dilatation with no evidence of ependymal sloughing or white matter damage (Fig. 1 E). Interestingly, *bgh* mutants on the 129 background present hydrocephalus with varying degrees of severity, ranging from mild enlargement of the ventricles to more severe ventricular dilatation and damage to the white matter, although ependymal sloughing was rarely observed (Fig. 1 F).

Defects in the ciliated ependymal cells lining the lateral ventricles were further investigated using an immunohistochemical approach. Staining for ciliary marker acetylated tubulin shows morphology consistent with the histological analysis. In the WT brains, the entire wall of the lateral ventricle is lined with organized cilia (Fig. 1 G, J, M, P). Both *nm1054* and *bgh* mutants on the 129 background also possess organized ciliated ependyma (Fig. 1 K, L, Q, R). Although there is occasional sloughing of the ependymal layer in the *bgh* mutants on the 129 background, the cilia largely remain intact (Fig. 1 L, R). In both mutants on the B6 background, however, there is extensive ependymal sloughing and loss of cilia along the surface of the lateral ventricles (Fig. 1 H, I, N, O).

Histological examination of the caudal regions of *nm1054* and *bgh* brains demonstrated dilatation of the third ventricle on the B6 background (Fig. 2 A-C). Consistent with the lateral ventricles, *bgh* mutants on the 129 background showed some dilatation, but little to no enlargement was observed in *nm1054* mutants on the 129 background (Fig. 2 D-F). Acetylated tubulin immunostaining indicates that the ciliated ependymal cells lining the third ventricle are intact in both mutants on both backgrounds (Fig.2 G-L). In addition, there is no evidence of dilatation, ependymal sloughing, or loss of cilia in the aqueduct of Sylvius (Fig. 3 A-L) or the fourth ventricle (Fig. 3 M-X) of either mutant on either background. Absence of obstructions or strictures in the ventricular system suggests that the hydrocephalus in *nm1054* and *bgh* mutants is due to a functional defect rather than an obstructive one.

3.2. *nm1054* and *bgh* mutants have strain-dependent glial responses

To further characterize the damage in *nm1054* and *bgh* brains, presence and organization of specific cell types were visualized using immunohistochemistry. Gliosis involves the activation and recruitment of several glial cell types, including astrocytes and microglia, in response to damage to the central nervous system (Burda and Sofroniew, 2014; Pekny et al., 2014). Activation of astrocytes, which play a critical role in synapse formation, control of neurotransmission, and regulation of cerebral blood flow, accompanies most central nervous system pathologies and has been associated with injury repair (Pekny et al., 2014). Up-regulation of the astrocytic intermediate filament protein glial fibrillary acidic protein (GFAP) is a hallmark of astrocytic activation (Pekny et al., 2014) and has been reported in models of hydrocephalus (Catalao et al., 2014; Di Curzio et al., 2013; Olopade et al., 2012; Xu et al., 2012a; Xu et al., 2012b). Analysis of GFAP shows only a low level of staining in WT mice (Fig. 4 A, D, G, J). However, *nm1054* and *bgh* mutants on the B6 background (Fig. 4 B, C, H, I) demonstrate a notable increase in staining, indicating a rise in astrocytic activation. GFAP expression in *nm1054* mice maintained on the 129 background is almost indistinguishable from the WT controls with a low level of staining present throughout and a slight enrichment of signal in the white matter tracts (Fig. 4 E, K). An increase in GFAP staining was observed in *bgh* mutants on the 129 background (Fig. 4 F, L), although the level of staining was variable in this population.

Microglia are macrophages that populate the central nervous system and play an important role in the neuroinflammatory response (Lyman et al., 2014). In the presence of cytokines and other signaling molecules released in response to acute inflammation, microglia transform from their inactive, ramified state to an active, phagocytic one (Lyman et al., 2014), and microglial activation has been shown to accompany the brain tissue damage associated with hydrocephalus (Di Curzio et al., 2013; Olopade et al., 2012; Xu et al., 2012a; Xu et al., 2012b). Staining for Iba1, a marker of all microglia (Ito et al., 1998), shows an increase in microglial cells in *nm1054* and *bgh* brains on the B6 background compared to WT (Fig. 4 M-O). In contrast, staining is lower in both mutants on the 129 background and is generally comparable to WT mice (Fig. 4 P-R). CD68 staining, which is indicative of activated microglia (Billiards et al., 2006), shows a similar increase in *nm1054* and *bgh* mutants on the B6 background (Fig. 4 S-U), whereas staining in the 129 mutants is generally similar to WT (Fig. 4 V-X). These findings indicate an increase in microglial presence and

activation in mutants on the B6 background that is indicative of a neuroinflammatory response in these brains.

3.3. *nm1054 and bgh* mutants have strain-dependent morphological changes in oligodendrocytes and neurons

Neural axons are wrapped in myelin, a sheath produced by oligodendrocytes that acts as an electrical insulator and greatly increases action potential speeds (Nave, 2010; Simons and Trotter, 2007). Myelin basic protein (MBP), a protein generally associated with the formation of myelin in oligodendrocytes, is elevated in the CSF of hydrocephalic patients (Beems et al., 2003; Longatti et al., 1993; Longatti et al., 1994; Naureen et al., 2013). Additionally, defects in myelination have been shown to result from hydrocephalus (Di Curzio et al., 2013; Goto et al., 2008; Hanlo et al., 1997). To examine whether myelination by oligodendrocytes is disrupted in the white matter of *nm1054* and *bgh* mutant mice, MBP expression was analyzed. In WT mice on both strains, staining is robust and highly organized (Fig. 5 A, D, G, J). The external capsule possesses a highly ordered structure, and axons clearly radiate from the fiber tracts into the cortex. In contrast, in both mutants on the B6 background, the white matter is disordered, and the radiating axons are absent (Fig. 5 B, C, H, I). On the 129 background, MBP staining in *nm1054* mutants is organized and similar to WT (Fig. 5 E, K), but the staining pattern is disorganized and more variable in the *bgh* mutants (Fig. 5 F, L). In addition, the corpus callosum is intact, but there is thinning and disorganization in both mutants on the B6 background compared to WT (Fig. 5 M-O).

Neuronal death has been reported in hydrocephalic patients and animal models (Castejon, 2010). Microtubule-associated protein 2 (MAP2) is a microtubule-binding protein expressed in the apical dendrites of cortical neurons (De Camilli et al., 1984). Recent evidence suggests that compression of the cortex decreases dendritic expression of MAP2 and drives expression back into the neuronal soma (Furutani and Kibayashi, 2012). Therefore, MAP2 staining was analyzed to investigate neuronal morphology in *nm1054* and *bgh* brains. Immunohistochemical staining for MAP2 in the WT cortex shows a visible pattern of fibers that radiate from the corpus callosum out to the surface of the brain (Fig. 6 A, D). In contrast, in both *nm1054* and *bgh* mutants on the B6 background, this pattern of radiating fibers is replaced by a more punctate staining of the cell soma (Fig. 6 B, C). This finding indicates that neuronal organization is altered in the mutant brains, likely due to cortical compression. MAP2 staining in *nm1054* brains from the 129 background is organized and similar to WT (Fig. 6 E). The pattern observed in *bgh* mutants on the 129 background is a variable combination of normal fibrous staining and disorganized punctate staining (Fig. 6 F). When combined, the histopathological and immunohistochemical data demonstrate substantial damage to *nm1054* and *bgh* brains on the B6 background compared to a mild (*nm1054*) or variable (*bgh*) morphological phenotype on the 129 background.

3.4. *nm1054* and *bgh* mutants exhibit decreased cilia function and CSF flow independent of genetic background

Based on the respiratory ciliary defect observed in both *nm1054* and *bgh* mice (Lee et al., 2008; Sironen et al., 2011), it is hypothesized that the hydrocephalus and associated morphological abnormalities are due to dysfunctional ependymal cilia. To assess ependymal

ciliary function in both mutants, cilia-driven flow was examined *ex vivo*. The lateral wall of the lateral ventricle was exposed by dissection, a small amount of ink was deposited onto the ependyma, and the stream of cilia-driven ink flow was observed over the course of two seconds. In WT mice, ink flowed in a reproducible stream over the rostral portion of the ependyma in a ventral direction (Fig. 7 A, B, G, H), which is consistent with a previous report (Sawamoto et al., 2006). Despite the presence of gross hydrocephalus and more severe morphological defects on the B6 background, flow of ink over mutant ependyma was visibly perturbed on both backgrounds (Fig. 7 C-F, I-L). Surprisingly, this defect was most severe over *bgh* ependyma on the 129 background, where there was no observable stream in the ventral direction (Fig. 7 K, L). Additionally, an abnormal flow pattern was observed over *bgh* ependyma, where there was a sideways movement of ink across the surface of the ventricle, compared to the defined stream that runs in the ventral direction along the rostral edge of WT ependyma (Fig. 7 M, N). This abnormal flow pattern was observed in all *bgh* mutants regardless of genetic background, suggesting that there is a defect in the coordination of ependymal ciliary beating in these mice.

Cilia-driven flow rates were calculated from the micrometer distance the ink traveled in the proper ventral direction over the course of two seconds (Fig. 7 O). Ink moved over WT ependyma at average rates of 193.75 and 160.25 μm/sec on the B6 and 129 backgrounds, respectively. On the B6 background, a significantly decreased flow rate of 75.40 μm/sec was observed over *bgh* ependyma, and a downward trend to 146.73 μm/sec was observed for *nm1054* mutants. On the 129 background, there was a statistically significant decrease in flow rate over *nm1054* ependyma to 41.38 μm/sec. With a complete absence of a defined ink stream in the ventral direction, the *bgh* mutants on the 129 background have a cilia-driven flow rate of 0 μm/sec, although there is ink movement in a sideways direction. These data demonstrate that the ependymal cilia-driven flow rate is decreased in *nm1054* mutants by approximately 24% on the B6 background and 74% on the 129 background. In *bgh* mutants, the flow rate is decreased by approximately 61% on the B6 background, and proper directional flow is entirely ablated on the 129 background. Unlike the morphological phenotype, this physiological defect is neither mild nor variable for either mutant on the 129 background.

To confirm that the defect in cilia-driven flow rate *ex vivo* correlates with a defect in CSF flow *in vivo*, one microliter of India ink was injected into the right lateral ventricle of live mice and allowed to flow through the ventricular system before euthanizing the mice one minute later. CSF flow was analyzed by assessing the presence of ink in coronal sections throughout the ventricular system of injected brains. Ink was observed in the lateral ventricle, aqueduct of Sylvius and fourth ventricle of all WT animals analyzed (Fig. 8 A-F). All *nm1054* and *bgh* mutants had ink in the lateral ventricles, but many mutants showed no evidence of ink reaching the caudal end of the aqueduct or the fourth ventricle on either the B6 or the 129 background (Fig. 8 G-R). The frequency of mutant mice with ink entering the rostral end of the aqueduct is decreased compared to those retaining ink in the lateral ventricles (Fig. 9 A, B). The frequency of mutants with ink reaching the caudal end of the aqueduct is further reduced (Fig. 9 C), and most mutants had no ink in the fourth ventricle (Fig. 9 D). Although there is variability on the 129 background, the ability of ink to flow

through to the fourth ventricle is impaired in both mutants on both genetic backgrounds. Taken together, the *in vivo* and *ex vivo* flow data suggest that CSF flow is impaired on both genetic backgrounds due to ependymal ciliary dysfunction that results from loss of either Pcdp1 or Spef2. Given that the gross hydrocephalus and morphological defects are generally more severe on the B6 background than 129, it is likely that abnormal cilia-driven CSF flow is not the only factor contributing to the severity of hydrocephalus in the *nm1054* and *bgh* models.

4. Discussion

Analysis of brains from *nm1054* and *bgh* mice has revealed a variety of defects in these two models of PCD, including ventricular dilatation, ependymal sloughing, increased gliosis, abnormal myelination by oligodendrocytes, and structural changes in cortical neurons. The tissue damage is likely due to intraventricular pressure exerted by CSF accumulating in the lateral ventricles. The severity of these phenotypes correlates with the severity of gross hydrocephalus and is generally greater on the B6 background. However, physiological analyses of ependymal ciliary function and CSF flow demonstrate a functional defect in *nm1054* and *bgh* mice on both the B6 and the 129 background that does not correlate with severity of gross hydrocephalus or the morphological abnormalities. These findings suggest that, although defects in ependymal cilia play a role in the development of congenital hydrocephalus, abnormal cilia-driven CSF flow is not the sole determinant of the hydrocephalus in these models. It is therefore likely that genetic modifiers influence the severity of CSF accumulation, ventricular dilatation, and subsequent morphological damage and play a role in neural development and function that is independent of ependymal cilia mechanics.

Analysis of *nm1054* and *bgh* brains uncovered notable variability between these models. The morphological defects in *bgh* mice are consistently severe on the B6 background, while the severity is variable on the 129 background. Similar variability was not observed in *nm1054* mice, in which the damage was uniformly more severe on the B6 background than on the 129 background, where *nm1054* brains generally resemble those from WT animals. In addition, we observed an altered directional flow of ink over exposed *bgh* ependyma *ex vivo* that was not observed for *nm1054* mice. The phenotypic differences between these models could be due to a combination of genetic contribution from the background strains and differences in the function of the Pcdp1 and Spef2 proteins. The severity of the *bgh* phenotype is consistent with a previously published analysis of *Streptococcus pneunomiae* challenge in the respiratory system that showed a more severe inflammatory response in *bgh* mutants than *nm1054* mutants (McKenzie et al., 2013). Although ciliary beat frequency is decreased by a comparable amount in both models (Lee et al., 2008; Sironen et al., 2011), it is possible that *bgh* respiratory cilia beat with an altered waveform, which would be consistent with the aberrant direction of ink flow over *bgh* ependyma in this study.

Analysis of CSF flow *in vivo* showed variability in the ability of ink to travel through the ventricular system in both mutants on the 129 background. This could be due to variability in exposure of cilia to the injected ink within the ventricular space, the presence or absence of ependymal cells, or the size of the ventricles into which a fixed volume of ink was

injected. However, the quantitative analysis of ink flow over exposed ependyma *ex vivo* confirms that *nm1054* and *bgh* mutants have a defect in cilia-driven flow. In this assay, ink was only deposited onto ventricular walls with intact ependyma to ensure proper contact with cilia. This analysis not only showed that flow is impaired in both mutants due to dysfunctional cilia, but it also demonstrated a dramatic and statistically significant decrease in flow rate on the 129 background.

The discovery that the *nm1054* and *bgh* hydrocephalus is more severe on the B6 background than 129 is consistent with other PCD models that also display a strain-dependent hydrocephalus severity (Lee, 2013). Mice with mutations in *Dpcd/DNA polλ* and *Stk36* both display severe gross hydrocephalus when maintained on the B6 background but only moderate hydrocephalus on a mixed B6/129 background (Kobayashi et al., 2002; Merchant et al., 2005; Vogel et al., 2010; Vogel et al., 2012). Similar findings were reported for mice with mutations in *adenylate kinase 7* (*Ak7*), which have a more severe hydrocephalus when maintained on the FVB/N background than a mixed B6/129 background (Fernandez-Gonzalez et al., 2009; Vogel et al., 2012). A number of other PCD models that have only been analyzed on a single background also support this phenotypic pattern by generally displaying notable hydrocephalus on the B6 background and mild or no hydrocephalus on the 129 background (Lee, 2013).

As strain-dependent severity is present in additional mouse models of hydrocephalus, this phenomenon is not specific to PCD. For example, deletion of the sixth Ig domain of the L1 cell adhesion molecule (L1CAM) on the 129 background resulted in lateral ventricles of a normal size, but backcrossing the mutation onto the B6 background resulted in progressively more severe hydrocephalus and, eventually, embryonic lethality (Itoh et al., 2004). Prior studies examining mice lacking fyn, a member of the src family of tyrosine kinases, did not report ventricular dilatation (Grant et al., 1992; Yagi et al., 1994), but backcrossing the mutation onto the B6 background resulted in notable hydrocephalus and premature death (Goto et al., 2008). The *Naglu* mouse, a model of the autosomal recessive lysosomal storage disorder mucopolysaccharidosis type III B, has a mutation in the gene encoding α-*N*-acetylglucosaminidase (Gografe et al., 2003). Phenotypic analysis of the *Naglu* mouse uncovered strain-dependent hydrocephalus that is more severe on the B6 background than on a mixed B6/129 background. In addition, the *fierce* mouse, which lacks the gene encoding the nuclear receptor Nr2e1, was analyzed on three different backgrounds: B6, 129P3/JEms, and B6129F1 (Young et al., 2002). Several developmental abnormalities were observed on all three backgrounds, but hydrocephalus was unique to the B6 animals. The strain-dependent nature of the hydrocephalus associated with these mouse models suggests that susceptibility to severe congenital hydrocephalus is generally influenced by genetic modifiers and supports the idea that the modifiers of the *nm1054* and *bgh* hydrocephalus do not play a direct role in ependymal ciliary function. Future studies are required to fully understand the role and identity of these modifiers and their impact on development of congenital hydrocephalus.

Acknowledgments

The authors thank Casey McKenzie for assistance with mouse husbandry and helpful discussions, Katherine Johnson for technical assistance, and Austin Reno and Olga Savinova for critical reading of the manuscript. The authors also thank Zaman Mirzadeh and Jill Weimer for assistance with technique development. This work was funded by the National Institute of General Medical Sciences (NIGMS) of the National Institutes of Health (NIH) (P20GM103620) and Sanford Research. Katherine Johnson was supported by the National Science Foundation (NSF) through a Research Experience for Undergraduates site (1262744). This work utilized resources from the Sanford Research Molecular Pathology Core and Imaging Core, both of which are supported by NIGMS (P20GM103548).

References

Afzelius BA. Cilia-related diseases. J Pathol. 2004; 204:470–7. [PubMed: 15495266]

Al-Dosari MS, Al-Owain M, Tulbah M, Kurdi W, Adly N, Al-Hemidan A, Masoodi TA, Albash B, Alkuraya FS. Mutation in MPDZ causes severe congenital hydrocephalus. J Med Genet. 2013; 50:54–8. [PubMed: 23240096]

Beems T, Simons KS, Van Geel WJ, De Reus HP, Vos PE, Verbeek MM. Serum- and CSF-concentrations of brain specific proteins in hydrocephalus. Acta Neurochir (Wien). 2003; 145:37–43. [PubMed: 12545260]

Berbari NF, O'Connor AK, Haycraft CJ, Yoder BK. The primary cilium as a complex signaling center. Curr Biol. 2009; 19:R526–35. [PubMed: 19602418]

Billiards SS, Haynes RL, Folkerth RD, Trachtenberg FL, Liu LG, Volpe JJ, Kinney HC. Development of microglia in the cerebral white matter of the human fetus and infant. J Comp Neurol. 2006; 497:199–208. [PubMed: 16705680]

Browd SR, Gottfried ON, Ragel BT, Kestle JR. Failure of cerebrospinal fluid shunts: part II: overdrainage, loculation, and abdominal complications. Pediatr Neurol. 2006a; 34:171–6. [PubMed: 16504785]

Browd SR, Ragel BT, Gottfried ON, Kestle JR. Failure of cerebrospinal fluid shunts: part I: Obstruction and mechanical failure. Pediatr Neurol. 2006b; 34:83–92. [PubMed: 16458818]

Burda JE, Sofroniew MV. Reactive gliosis and the multicellular response to CNS damage and disease. Neuron. 2014; 81:229–48. [PubMed: 24462092]

Castejon OJ. Submicroscopic pathology of human and experimental hydrocephalic cerebral cortex. Folia Neuropathol. 2010; 48:159–74. [PubMed: 20925000]

Catalao CH, Correa DA, Saito ST, Lopes Lda S. Camellia sinensis neuroprotective role in experimentally induced hydrocephalus in Wistar rats. Childs Nerv Syst. 2014; 30:591–7. [PubMed: 24005799]

Chiafery M. Care and management of the child with shunted hydrocephalus. Pediatr Nurs. 2006; 32:222–5. [PubMed: 16802679]

Chodhari R, Mitchison HM, Meeks M. Cilia, primary ciliary dyskinesia and molecular genetics. Paediatr Respir Rev. 2004; 5:69–76. [PubMed: 15222957]

De Camilli P, Miller PE, Navone F, Theurkauf WE, Vallee RB. Distribution of microtubule-associated protein 2 in the nervous system of the rat studied by immunofluorescence. Neuroscience. 1984; 11:817–46. [PubMed: 6377119]

Del Bigio MR. Pathophysiologic consequences of hydrocephalus. Neurosurg Clin N Am. 2001; 12:639–49. vii. [PubMed: 11524286]

Del Bigio MR. Cellular damage and prevention in childhood hydrocephalus. Brain Pathol. 2004; 14:317–24. [PubMed: 15446588]

Di Curzio DL, Buist RJ, Del Bigio MR. Reduced subventricular zone proliferation and white matter damage in juvenile ferrets with kaolin-induced hydrocephalus. Exp Neurol. 2013; 248:112–28. [PubMed: 23769908]

DiPetrillo CG, Smith EF. Pcdp1 is a central apparatus protein that binds Ca(2+)- calmodulin and regulates ciliary motility. J Cell Biol. 2010; 189:601–12. [PubMed: 20421426]

Dominguez-Pinos MD, Paez P, Jimenez AJ, Weil B, Arraez MA, Perez-Figares JM, Rodriguez EM. Ependymal denudation and alterations of the subventricular zone occur in human fetuses with a

moderate communicating hydrocephalus. J Neuropathol Exp Neurol. 2005; 64:595–604. [PubMed: 16042311]

Drake JM. The surgical management of pediatric hydrocephalus. Neurosurgery. 2008; 62(Suppl 2): 633–40. discussion 640-2. [PubMed: 18596441]

Ekici AB, Hilfinger D, Jatzwauk M, Thiel CT, Wenzel D, Lorenz I, Boltshauser E, Goecke TW, Staatz G, Morris-Rosendahl DJ, Sticht H, Hehr U, Reis A, Rauch A. Disturbed Wnt Signalling due to a Mutation in CCDC88C Causes an Autosomal Recessive Non-Syndromic Hydrocephalus with Medial Diverticulum. Mol Syndromol. 2010; 1:99–112. [PubMed: 21031079]

Falcao AS, Silva RF, Vaz AR, Silva SL, Fernandes A, Brites D. Cross-talk between neurons and astrocytes in response to bilirubin: early beneficial effects. Neurochem Res. 2013; 38:644–59. [PubMed: 23283699]

Fernandez-Gonzalez A, Kourembanas S, Wyatt TA, Mitsialis SA. Mutation of murine adenylate kinase 7 underlies a primary ciliary dyskinesia phenotype. Am J Respir Cell Mol Biol. 2009; 40:305–13. [PubMed: 18776131]

Furutani R, Kibayashi K. Morphological alteration and reduction of MAP2- immunoreactivity in pyramidal neurons of cerebral cortex in a rat model of focal cortical compression. J Neurotrauma. 2012; 29:1266–76. [PubMed: 21401443]

Gografe SI, Garbuzova-Davis S, Willing AE, Haas K, Chamizo W, Sanberg PR. Mouse model of Sanfilippo syndrome type B: relation of phenotypic features to background strain. Comp Med. 2003; 53:622–32. [PubMed: 14727810]

Goto J, Tezuka T, Nakazawa T, Sagara H, Yamamoto T. Loss of Fyn tyrosine kinase on the C57BL/6 genetic background causes hydrocephalus with defects in oligodendrocyte development. Mol Cell Neurosci. 2008; 38:203–12. [PubMed: 18403215]

Grant SG, O'Dell TJ, Karl KA, Stein PL, Soriano P, Kandel ER. Impaired long-term potentiation, spatial learning, and hippocampal development in fyn mutant mice. Science. 1992; 258:1903–10. [PubMed: 1361685]

Guemez-Gamboa A, Coufal NG, Gleeson JG. Primary Cilia in the Developing and Mature Brain. Neuron. 2014; 82:511–521. [PubMed: 24811376]

Hanigan WC, Morgan A, Shaaban A, Bradle P. Surgical treatment and long-term neurodevelopmental outcome for infants with idiopathic aqueductal stenosis. Childs Nerv Syst. 1991; 7:386–90. [PubMed: 1724411]

Hanlo PW, Gooskens RJ, van Schooneveld M, Tulleken CA, van der Knaap MS, Faber JA, Willemse J. The effect of intracranial pressure on myelination and the relationship with neurodevelopment in infantile hydrocephalus. Dev Med Child Neurol. 1997; 39:286–91. [PubMed: 9236693]

Horani A, Brody SL, Ferkol TW. Picking up speed: advances in the genetics of primary ciliary dyskinesia. Pediatr Res. 2014; 75:158–64. [PubMed: 24192704]

Ibanez-Tallon I, Heintz N, Omran H. To beat or not to beat: roles of cilia in development and disease. Hum Mol Genet. 2003; 12(Spec No 1):R27–35. [PubMed: 12668594]

Ito D, Imai Y, Ohsawa K, Nakajima K, Fukuuchi Y, Kohsaka S. Microglia-specific localisation of a novel calcium binding protein, Iba1. Brain Res Mol Brain Res. 1998; 57:1–9. [PubMed: 9630473]

Itoh K, Cheng L, Kamei Y, Fushiki S, Kamiguchi H, Gutwein P, Stoeck A, Arnold B, Altevogt P, Lemmon V. Brain development in mice lacking L1-L1 homophilic adhesion. J Cell Biol. 2004; 165:145–54. [PubMed: 15067019]

Jouet M, Rosenthal A, MacFarlane J, Kenwrick S, Donnai D. A missense mutation confirms the L1 defect in X-linked hydrocephalus (HSAS). Nat Genet. 1993; 4:331. [PubMed: 8401576]

Kang JK, Lee IW. Long-term follow-up of shunting therapy. Childs Nerv Syst. 1999; 15:711–7. [PubMed: 10603012]

Khan AA, Jabbar A, Banerjee A, Hinchley G. Cerebrospinal shunt malfunction: recognition and emergency management. Br J Hosp Med (Lond). 2007; 68:651–5. [PubMed: 18186399]

Knowles MR, Daniels LA, Davis SD, Zariwala MA, Leigh MW. Primary ciliary dyskinesia. Recent advances in diagnostics, genetics, and characterization of clinical disease. Am J Respir Crit Care Med. 2013; 188:913–22. [PubMed: 23796196]

Kobayashi Y, Watanabe M, Okada Y, Sawa H, Takai H, Nakanishi M, Kawase Y, Suzuki H, Nagashima K, Ikeda K, Motoyama N. Hydrocephalus, situs inversus, chronic sinusitis, and male

infertility in DNA polymerase lambda-deficient mice: possible implication for the pathogenesis of immotile cilia syndrome. Mol Cell Biol. 2002; 22:2769–76. [PubMed: 11909969]

Lambe T, Simpson RJ, Dawson S, Bouriez-Jones T, Crockford TL, Lepherd M, Latunde-Dada GO, Robinson H, Raja KB, Campagna DR, Villarreal G Jr, Ellory JC, Goodnow CC, Fleming MD, McKie AT, Cornall RJ. Identification of a Steap3 endosomal targeting motif essential for normal iron metabolism. Blood. 2009; 113:1805–8. [PubMed: 18955558]

Lee L. Mechanisms of mammalian ciliary motility: Insights from primary ciliary dyskinesia genetics. Gene. 2011; 473:57–66. [PubMed: 21111794]

Lee L. Riding the wave of ependymal cilia: Genetic susceptibility to hydrocephalus in primary ciliary dyskinesia. J Neurosci Res. 2013; 91:1117–32. [PubMed: 23686703]

Lee L, Campagna DR, Pinkus JL, Mulhern H, Wyatt TA, Sisson JH, Pavlik JA, Pinkus GS, Fleming MD. Primary ciliary dyskinesia in mice lacking the novel ciliary protein Pcdp1. Mol Cell Biol. 2008; 28:949–57. [PubMed: 18039845]

Lee L, DeBono CA, Campagna DR, Young DC, Moody DB, Fleming MD. Loss of the acyl-CoA binding protein (Acbp) results in fatty acid metabolism abnormalities in mouse hair and skin. J Invest Dermatol. 2007; 127:16–23. [PubMed: 16902415]

Leigh MW, Pittman JE, Carson JL, Ferkol TW, Dell SD, Davis SD, Knowles MR, Zariwala MA. Clinical and genetic aspects of primary ciliary dyskinesia/Kartagener syndrome. Genet Med. 2009; 11:473–87. [PubMed: 19606528]

Longatti PL, Canova G, Guida F, Carniato A, Moro M, Carteri A. The CSF myelin basic protein: a reliable marker of actual cerebral damage in hydrocephalus. J Neurosurg Sci. 1993; 37:87–90. [PubMed: 7507986]

Longatti PL, Guida F, Agostini S, Carniato B, Carteri A. The CSF myelin basic protein in pediatric hydrocephalus. Childs Nerv Syst. 1994; 10:96–8. [PubMed: 7518354]

Lyman M, Lloyd DG, Ji X, Vizcaychipi MP, Ma D. Neuroinflammation: The role and consequences. Neurosci Res. 2014; 79C:1–12. [PubMed: 24144733]

Markakis EA, Sasaki M, Lankford KL, Kocsis JD. Convergence of cells from the progenitor fraction of adult olfactory bulb tissue to remyelinating glia in demyelinating spinal cord lesions. PLoS One. 2009; 4:e7260. [PubMed: 19787061]

Mataro M, Junque C, Poca MA, Sahuquillo J. Neuropsychological findings in congenital and acquired childhood hydrocephalus. Neuropsychol Rev. 2001; 11:169–78. [PubMed: 11883667]

McKenzie CW, Klonoski JM, Maier T, Trujillo G, Vitiello PF, Huber VC, Lee L. Enhanced response to pulmonary Streptococcus pneumoniae infection is associated with primary ciliary dyskinesia in mice lacking Pcdp1 and Spef2. Cilia. 2013; 2:18. [PubMed: 24360193]

Merchant M, Evangelista M, Luoh SM, Frantz GD, Chalasani S, Carano RA, van Hoy M, Ramirez J, Ogasawara AK, McFarland LM, Filvaroff EH, French DM, de Sauvage FJ. Loss of the serine/threonine kinase fused results in postnatal growth defects and lethality due to progressive hydrocephalus. Mol Cell Biol. 2005; 25:7054–68. [PubMed: 16055717]

Mirzadeh Z, Doetsch F, Sawamoto K, Wichterle H, Alvarez-Buylla A. The subventricular zone en-face: wholemount staining and ependymal flow. J Vis Exp. 2010

Naureen I, Waheed KA, Rathore AW, Victor S, Mallucci C, Goodden JR, Chohan SN, Miyan JA. Fingerprint changes in CSF composition associated with different aetiologies in human neonatal hydrocephalus: glial proteins associated with cell damage and loss. Fluids Barriers CNS. 2013; 10:34. [PubMed: 24351234]

Nave KA. Myelination and support of axonal integrity by glia. Nature. 2010; 468:244–52. [PubMed: 21068833]

Ohgami RS, Campagna DR, Antiochos B, Wood EB, Sharp JJ, Barker JE, Fleming MD. nm1054: a spontaneous, recessive, hypochromic, microcytic anemia mutation in the mouse. Blood. 2005a; 106:3625–31. [PubMed: 15994289]

Ohgami RS, Campagna DR, Greer EL, Antiochos B, McDonald A, Chen J, Sharp JJ, Fujiwara Y, Barker JE, Fleming MD. Identification of a ferrireductase required for efficient transferrin-dependent iron uptake in erythroid cells. Nat Genet. 2005b; 37:1264–1269. [PubMed: 16227996]

Olopade FE, Shokunbi MT, Siren AL. The relationship between ventricular dilatation, neuropathological and neurobehavioural changes in hydrocephalic rats. Fluids Barriers CNS. 2012; 9:19. [PubMed: 22938200]

Pekny M, Wilhelmsson U, Pekna M. The dual role of astrocyte activation and reactive gliosis. Neurosci Lett. 2014

Perez-Figares JM, Jimenez AJ, Rodriguez EM. Subcommissural organ, cerebrospinal fluid circulation, and hydrocephalus. Microsc Res Tech. 2001; 52:591–607. [PubMed: 11241868]

Rekate HL. Recent advances in the understanding and treatment of hydrocephalus. Semin Pediatr Neurol. 1997; 4:167–78. [PubMed: 9323787]

Rekate HL. A consensus on the classification of hydrocephalus: its utility in the assessment of abnormalities of cerebrospinal fluid dynamics. Childs Nerv Syst. 2011; 27:1535–41. [PubMed: 21928019]

Satir P, Christensen ST. Overview of structure and function of mammalian cilia. Annu Rev Physiol. 2007; 69:377–400. [PubMed: 17009929]

Sawamoto K, Wichterle H, Gonzalez-Perez O, Cholfin JA, Yamada M, Spassky N, Murcia NS, Garcia-Verdugo JM, Marin O, Rubenstein JL, Tessier-Lavigne M, Okano H, Alvarez-Buylla A. New neurons follow the flow of cerebrospinal fluid in the adult brain. Science. 2006; 311:629–32. [PubMed: 16410488]

Simons M, Trotter J. Wrapping it up: the cell biology of myelination. Curr Opin Neurobiol. 2007; 17:533–40. [PubMed: 17923405]

Sironen A, Hansen J, Thomsen B, Andersson M, Vilkki J, Toppari J, Kotaja N. Expression of SPEF2 during mouse spermatogenesis and identification of IFT20 as an interacting protein. Biol Reprod. 2010; 82:580–90. [PubMed: 19889948]

Sironen A, Kotaja N, Mulhern H, Wyatt TA, Sisson JH, Pavlik JA, Miiluniemi M, Fleming MD, Lee L. Loss of SPEF2 Function in Mice Results in Spermatogenesis Defects and Primary Ciliary Dyskinesia. Biol Reprod. 2011; 85:690–701. [PubMed: 21715716]

Sironen A, Thomsen B, Andersson M, Ahola V, Vilkki J. An intronic insertion in KPL2 results in aberrant splicing and causes the immotile short-tail sperm defect in the pig. Proc Natl Acad Sci U S A. 2006; 103:5006–11. [PubMed: 16549801]

Srivastava DP, Woolfrey KM, Jones KA, Anderson CT, Smith KR, Russell TA, Lee H, Yasvoina MV, Wokosin DL, Ozdinler PH, Shepherd GM, Penzes P. An autism-associated variant of Epac2 reveals a role for Ras/Epac2 signaling in controlling basal dendrite maintenance in mice. PLoS Biol. 2012; 10:e1001350. [PubMed: 22745599]

Steffenhagen C, Dechant FX, Oberbauer E, Furtner T, Weidner N, Kury P, Aigner L, Rivera FJ. Mesenchymal stem cells prime proliferating adult neural progenitors toward an oligodendrocyte fate. Stem Cells Dev. 2012; 21:1838–51. [PubMed: 22074360]

Thelen M, Damme M, Schweizer M, Hagel C, Wong AM, Cooper JD, Braulke T, Galliciotti G. Disruption of the autophagy-lysosome pathway is involved in neuropathology of the nclf mouse model of neuronal ceroid lipofuscinosis. PLoS One. 2012; 7:e35493. [PubMed: 22536393]

Vogel P, Read R, Hansen GM, Freay LC, Zambrowicz BP, Sands AT. Situs inversus in Dpcd/Poll-/-, Nme7-/- , and Pkd1l1-/- mice. Vet Pathol. 2010; 47:120–31. [PubMed: 20080492]

Vogel P, Read RW, Hansen GM, Payne BJ, Small D, Sands AT, Zambrowicz BP. Congenital hydrocephalus in genetically engineered mice. Vet Pathol. 2012; 49:166–81. [PubMed: 21746835]

Wallingford JB. Planar cell polarity signaling, cilia and polarized ciliary beating. Curr Opin Cell Biol. 2010; 22:597–604. [PubMed: 20817501]

Woodruff TM, Costantini KJ, Crane JW, Atkin JD, Monk PN, Taylor SM, Noakes PG. The complement factor C5a contributes to pathology in a rat model of amyotrophic lateral sclerosis. J Immunol. 2008; 181:8727–34. [PubMed: 19050293]

Xu H, Tan G, Zhang S, Zhu H, Liu F, Huang C, Zhang F, Wang Z. Minocycline reduces reactive gliosis in the rat model of hydrocephalus. BMC Neurosci. 2012a; 13:148. [PubMed: 23217034]

Xu H, Zhang SL, Tan GW, Zhu HW, Huang CQ, Zhang FF, Wang ZX. Reactive gliosis and neuroinflammation in rats with communicating hydrocephalus. Neuroscience. 2012b; 218:317–25. [PubMed: 22583796]

Yagi T, Shigetani Y, Furuta Y, Nada S, Okado N, Ikawa Y, Aizawa S. Fyn expression during early neurogenesis in mouse embryos. Oncogene. 1994; 9:2433–40. [PubMed: 8058305]

Young KA, Berry ML, Mahaffey CL, Saionz JR, Hawes NL, Chang B, Zheng QY, Smith RS, Bronson RT, Nelson RJ, Simpson EM. Fierce: a new mouse deletion of Nr2e1; violent behaviour and ocular abnormalities are background-dependent. Behav Brain Res. 2002; 132:145–58. [PubMed: 11997145]

Zhang H, Mitchell DR. Cpcl, a Chlamydomonas central pair protein with an adenylate kinase domain. J Cell Sci. 2004; 117:4179–88. [PubMed: 15292403]

Zhang J, Williams MA, Rigamonti D. Genetics of human hydrocephalus. J Neurol. 2006; 253:1255–66. [PubMed: 16773266]

Abbreviations

129	129S6/SvEvTac
B6	C57BL/6J
Ak7	adenylate kinase 7
bgh	big giant head
CCDC88C	coiled coil domain containing 88C
Cfap221	ciliary and flagellar associated protein 221
Cpc1	central pair complex 1
CSF	cerebrospinal fluid
Dpcd	deleted in primary ciliary dyskinesia
GFAP	glial fibrillary acidic protein
H&E	hematoxylin and eosin
Iba1	ionized calcium binding adapter molecule 1
L1CAM	L1 cell adhesion molecule
MAP2	microtubule-associated protein 2
MBP	myelin basic protein
MPDZ	multiple PDZ domain protein
nm1054	the 1054^{th} new mutation described at the Jackson Labs
PCD	primary ciliary dyskinesia
Pcdp1	primary ciliary dyskinesia protein 1
Spef2	sperm flagellar protein 2
Stk36	serine/threonine kinase 36
WT	wild type

Highlights

- Mice lacking *Pcdp1* and *Spef2* have hydrocephalus with damage to multiple cell types
- Morphological defects are more severe on the C57BL/6J background than 29S6/SvEvTac
- Mutants have a defect in cilia-driven cerebrospinal fluid flow on both strains
- Genetic modifiers likely influence the severity of hydrocephalus in these models

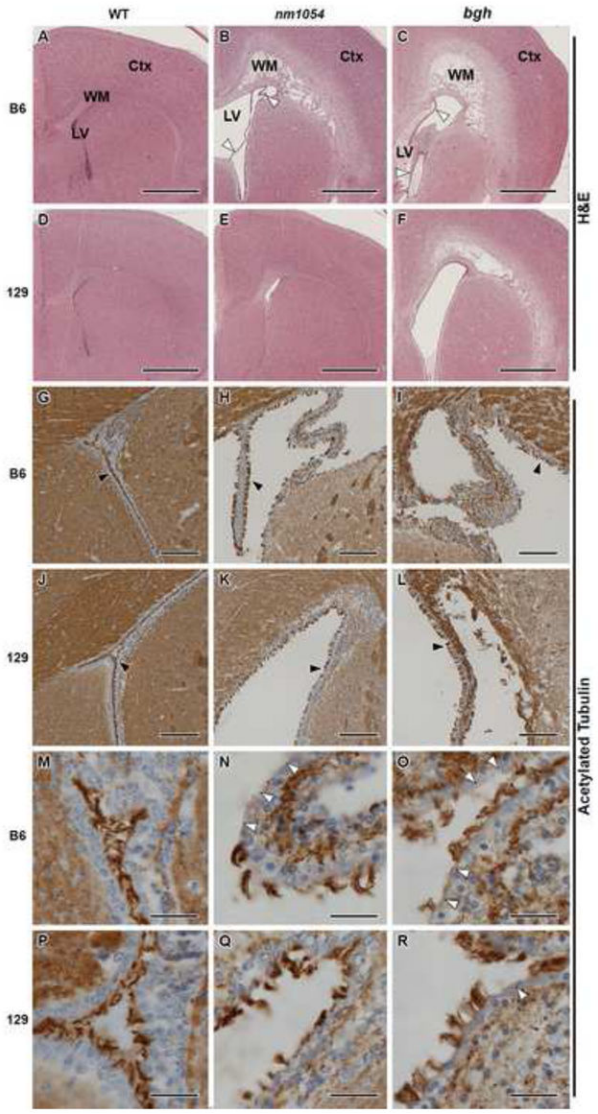

Figure 1. Morphological defects in *nm1054* and *bgh* lateral ventricles

(A-F) H&E staining of coronal sections through the lateral ventricles (LV) of WT (A, D), *nm1054* (B, E), and *bgh* (C, F) brains on the B6 (A-C) and 129 (D-F) backgrounds. Ventricular dilatation, sloughing of the ependyma (arrowheads), and physical damage to the white matter (WM) and cortex (Ctx) are observed in both mutants and are generally more severe on the B6 background. (G-R) Acetylated tubulin staining of coronal sections through the lateral ventricles of WT (G, J, M, P), *nm1054* (H, K, N, Q), and *bgh* (I, L, O, R) mice maintained on the B6 (G-I, M-O) and 129 (J-L, P-R) backgrounds demonstrates sloughing of ependymal cells and damage to the cilia in both mutants, which are generally more severe on the B6 background. Closed arrowheads indicate the presence of cilia; open arrowheads indicate loss of cilia. Representative images are shown. Scale bars represent 1 mm (A-F), 100 μm (G-L), and 25μm (M-R).

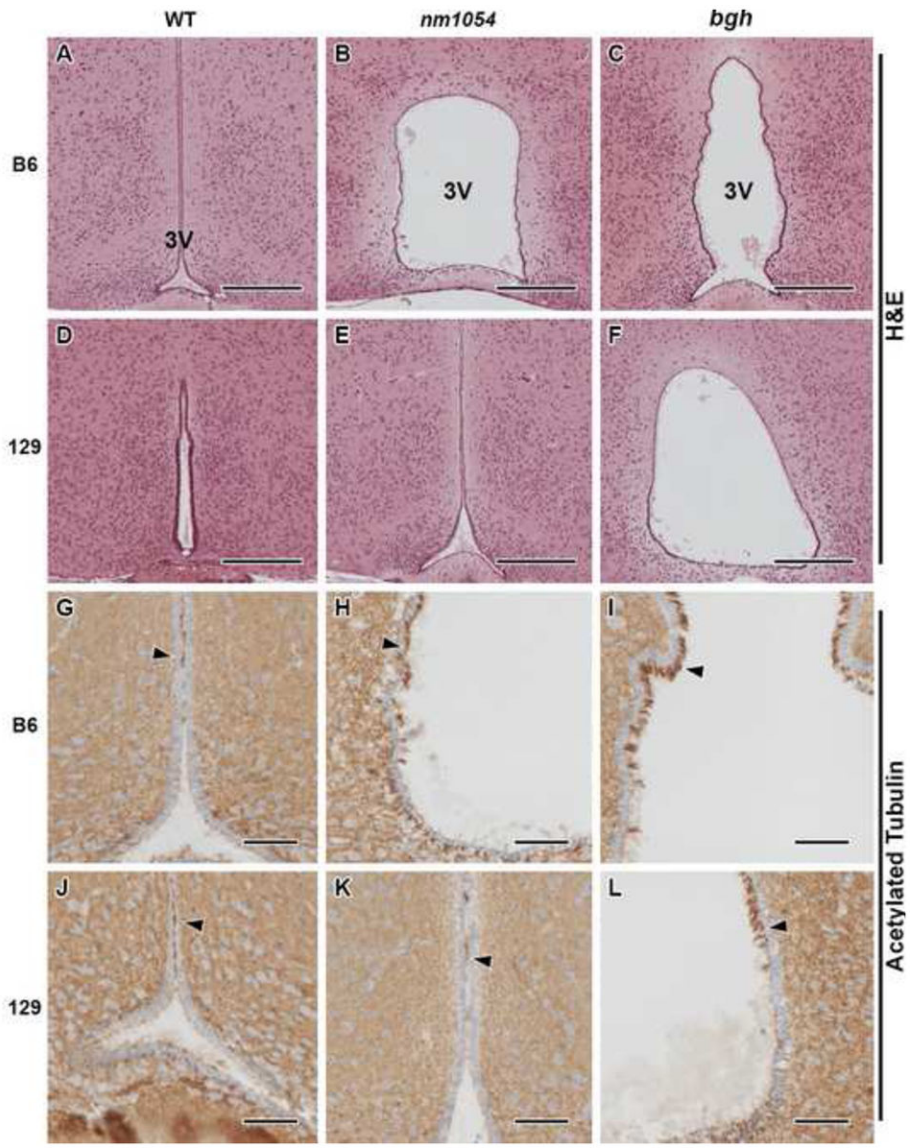

Figure 2. Morphological defects in the *nm1054* and *bgh* third ventricle

(A-F) H&E staining of coronal sections through the third ventricle (3V) of WT (A, D), *nm1054* (B, E), and *bgh* (C, F) brains on the B6 (A-C) and 129 (D-F) backgrounds. Ventricular dilatation is present in both mutants on the B6 background, as well as *bgh* animals on the 129 background, with no evidence of ependymal sloughing or tissue damage. (G-L) Acetylated tubulin staining of coronal sections through the third ventricle of WT (G, J), *nm1054* (H, K), and *bgh* (I, L) mice on the B6 (G-I) and 129 (J-L) backgrounds demonstrates that the ciliated ependymal cells are intact and undamaged. Cilia are indicated by arrowheads. Representative images are shown. Scale bars represent 250 μm (A-F) and 50 μm (G-L).

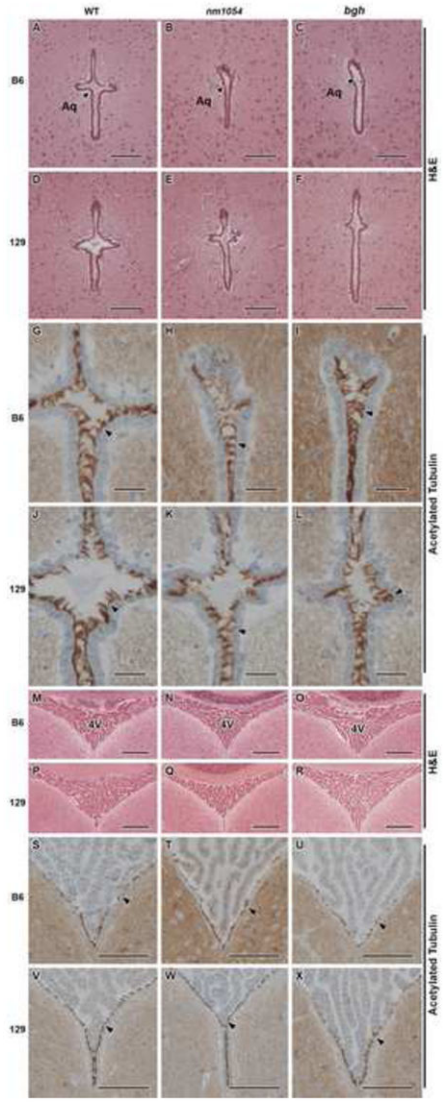

Figure 3. Morphological defects in the *nm1054* and *bgh* aqueduct and fourth ventricle

(A-F) H&E staining of coronal sections through the aqueduct of Sylvius (Aq) of WT (A, D), *nm1054* (B, E), and *bgh* (C, F) brains on the B6 (A-C) and 129 (D-F) backgrounds indicating no dilatation, ependymal sloughing, tissue damage, or constriction. (G-L) Acetylated tubulin staining of coronal sections through the aqueduct of WT (G, J), *nm1054* (H, K), and *bgh* (I, L) mice on the B6 (G-I) and 129 (J-L) backgrounds demonstrates that ciliated ependymal cells are intact and undamaged. (M-R) H&E staining of coronal sections through the fourth ventricle (4V) of WT (M, P), *nm1054* (N, Q), and *bgh* (O, R) brains on the B6 (M-O) and 129 (P-R) backgrounds indicating no dilatation, ependymal sloughing, or tissue damage. (S-X) Acetylated tubulin staining of coronal sections through the fourth ventricle of WT (S, V), *nm1054* (T, W), and *bgh* (U, X) mice on the B6 (S-U) and 129 (V-X) backgrounds demonstrates that ciliated ependymal cells are intact and undamaged. Cilia are indicated by arrowheads. Representative images are shown. Scale bars represent 100 μm (A-F, S-X), 25 μm (G-L), and 250 μm (M-R).

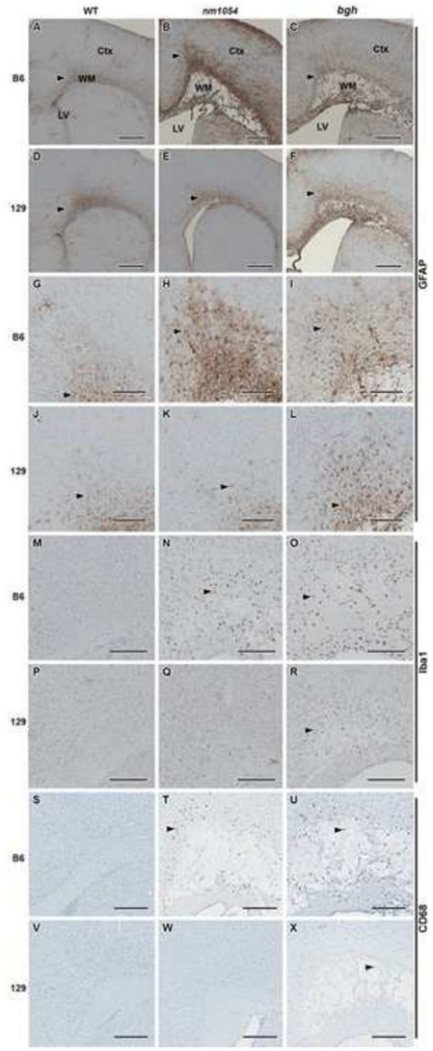

Figure 4. Increased gliosis in *nm1054* and *bgh* mutants

Staining for glial cell markers on coronal sections through the cerebral cortex (Ctx) and white matter (WM) dorsal to the lateral ventricles (LV). (A-L) GFAP staining for astrocytes in WT (A, D, G, J), *nm1054* (B, E, H, K), and *bgh* (C, F, I, L) brains on the B6 (A-C, G-I) and 129 (D-F, J-L) backgrounds. (M-R) Iba1 staining for microglia in WT (M, P), *nm1054* (N, Q), and *bgh* (O, R) brains on the B6 (M-O) and 129 (P-R) backgrounds. (S-X) CD68 staining for activated microglia in WT (S, V), *nm1054* (T, W), and *bgh* (U, X) mice on the B6 (S-U) and 129 (V-X) backgrounds. There is a notable increase in all glial cell populations in both mutants on the B6 background. Stained cells are indicated by arrowheads. Representative images are shown. Scale bars represent 500 μm (A-F), 200 μm (G-L), and 250 μm (M-X).

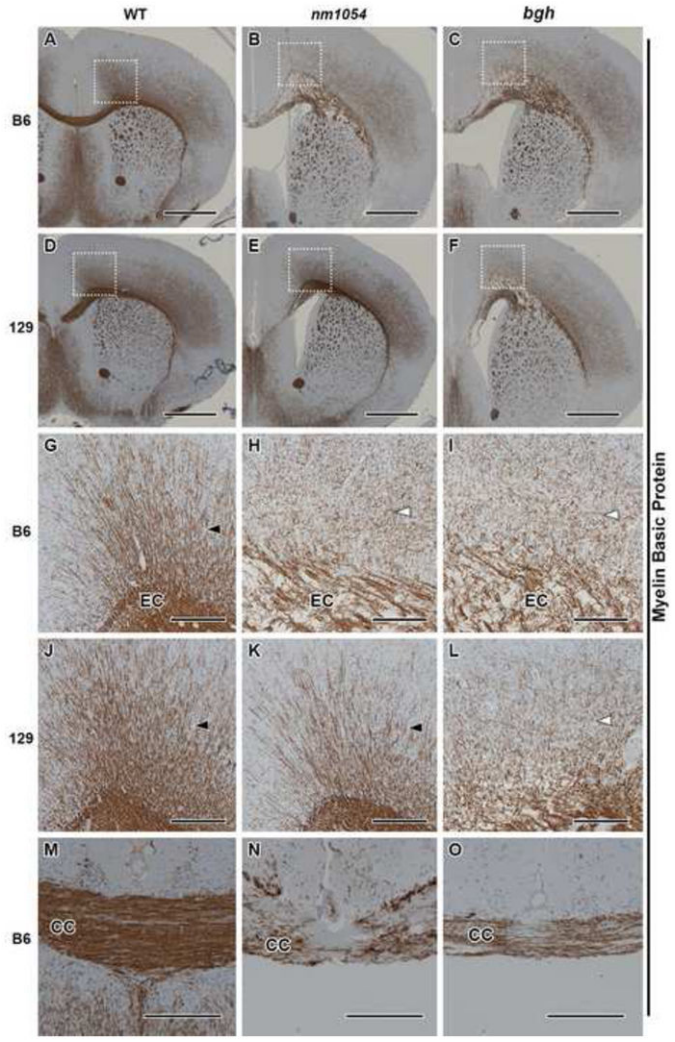

Figure 5. Disorganization of oligodendrocytes in *nm1054* and *bgh* mutants

Staining for oligodendrocyte marker MBP on coronal sections through the lateral ventricles. (A-F) Low magnification images of WT (A, D), *nm1054* (B, E), and *bgh* (C, F) brains on the B6 (A-C) and 129 (D-F) backgrounds. White boxes in A-F indicate the approximate location of the high magnification images in G-L. (G-L) High magnification images of the cerebral cortex dorsal to the lateral ventricles of WT (G, J), *nm1054* (H, K), and *bgh* (I, L) brains on the B6 (G-I) and 129 (J-L) backgrounds. WT brains have organized fiber tracts and a distinct external capsule (EC) with axons (closed arrowhead) radiating from the fiber tracts into the cortex, whereas both mutants have a disorganized external capsule and an absence of radiating axons (open arrowhead) that are generally more severe on the B6 background. (M-O) High magnification images of the corpus callosum (CC) at the midline in WT (M), *nm1054* (N), and *bgh* (O) brains on the B6 background show thinning and disorganization in both mutants. Representative images are shown. Scale bars represent 1 mm (A-F) and 200 μm (G-O).

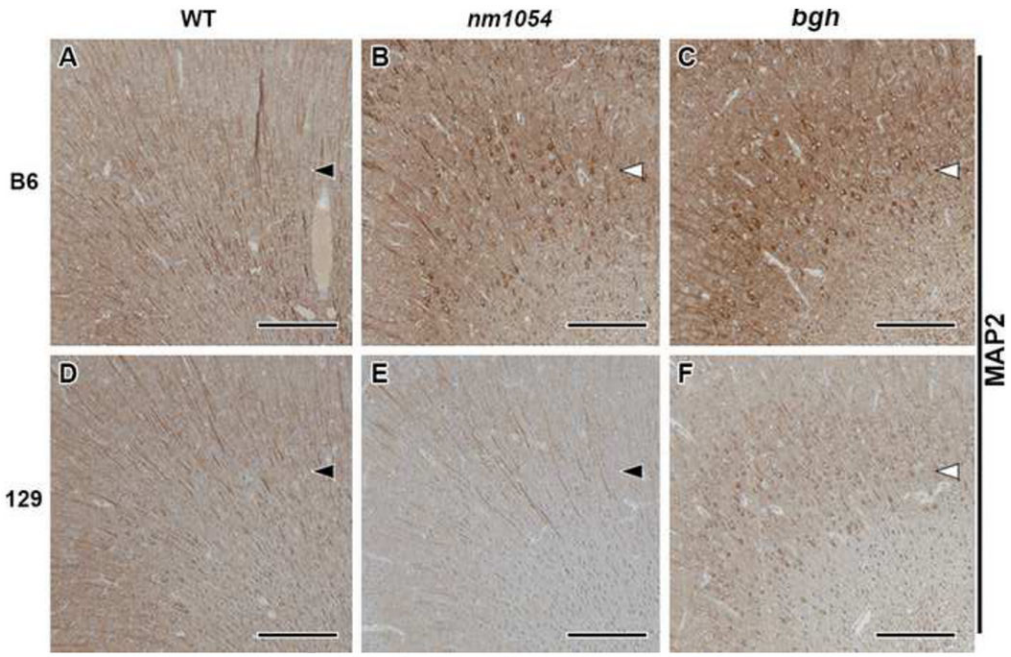

Figure 6. Aberrant morphology of cortical neurons in *nm1054* and *bgh* mutants

Staining for cortical neuron marker MAP2 on coronal sections through the cerebral cortex dorsal to the lateral ventricles of WT (A, D), *nm1054* (B, E), and *bgh* (C, F) mice on the B6 (A-C) and 129 (D-F) backgrounds. WT brains show a pattern of fibers radiating from the fiber tract (closed arrowhead), while the mutants show a more punctate staining of the cell soma (open arrowhead) that is generally more pronounced on the B6 background. Representative images are shown. Scale bars represent 200 μm.

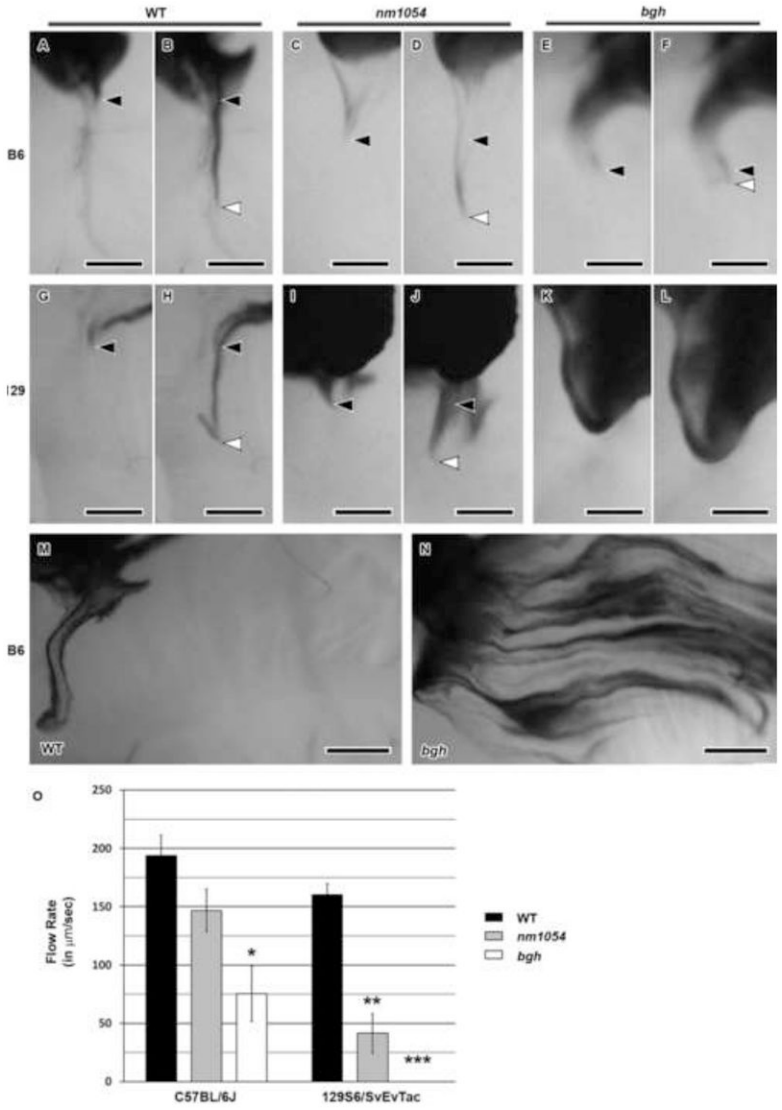

Figure 7. Ependymal cilia function is impaired in *nm1054* and *bgh* mutants

(A-L) Flow of ink was observed *ex vivo* on exposed ependyma from WT (A, B, G, H), *nm1054* (C, D, I, J), and *bgh* (E, F, K, L) mice on the B6 (A-F) and 129 (G-L) backgrounds. Images represent time 0 (A, C, E, G, I, K) and 2 seconds (B, D, F, H, J, L). Closed arrowheads denote the starting point of the ink stream, and open arrowheads indicate the position of the ink after two seconds. There was no observable cilia-driven ink movement in *bgh* mutants on the 129 background in the proper ventral direction (K, L), where only ink diffusion was observed. Representative images are shown. Scale bars represent 250 μm. (M, N) Aberrant directional flow over ependyma from *bgh* mutants (N) compared to WT (M). The brains shown in M and N are from B6 mice, although the *bgh* mutants displayed aberrant flow regardless of genetic background. Representative images are shown. Scale bars represent 500 μm. (O) Analysis of ink flow rate (microns/second) over exposed ependyma from WT, *nm1054*, and *bgh* lateral ventricles *ex vivo* indicates that cilia-driven flow is impaired in both mutants on both the B6 and the 129 backgrounds. Due to an absence of proper directional flow, the *bgh* flow rate on the 129 background is zero. Error

bars indicate standard error of the mean. Significance compared to WT was determined by two-tailed t test (* $p<0.005$, ** $p<0.0005$, *** $p<0.00005$).

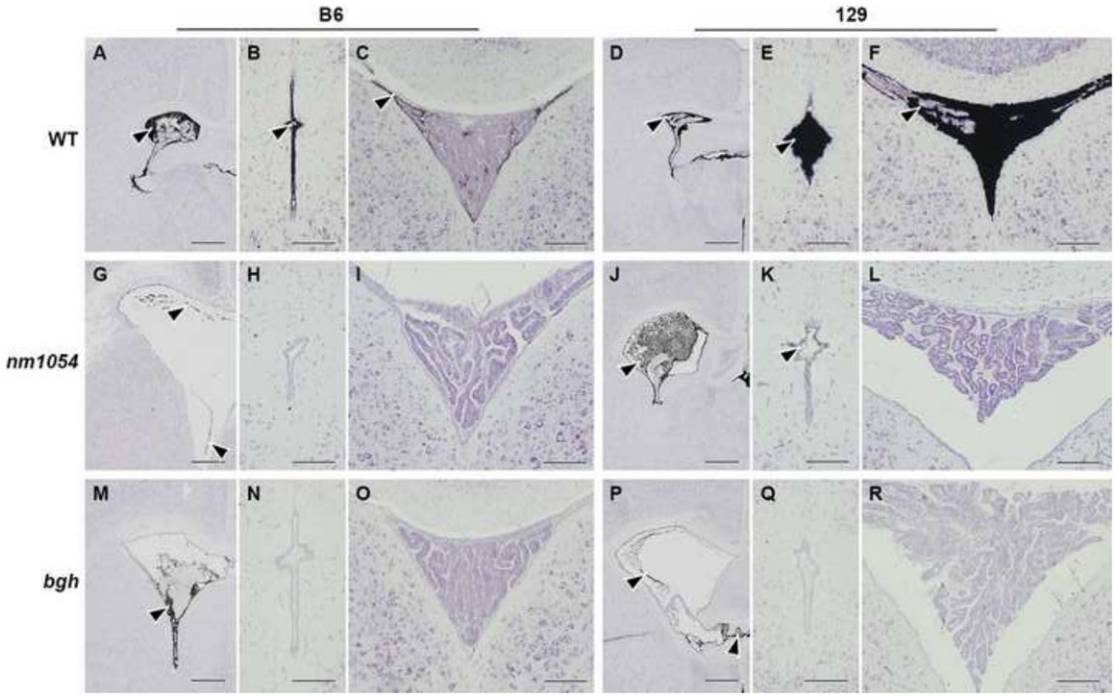

Figure 8. ***In vivo*** **CSF flow is impaired in** ***nm1054*** **and** ***bgh*** **mutants**

Coronal sections through the lateral ventricles (A, D, G, J, M, P), aqueduct of Sylvius (B, E, H, K, N, Q), and fourth ventricle (C, F, I, L, O, R) of WT (A-F), *nm1054* (G-L), and *bgh* (M-R) mice on the B6 (A-C, G-I, M-O) and 129 (D-F, J-L, P-R) backgrounds after injection of India ink into the lateral ventricles. Sections were stained with cresyl violet. Arrowheads indicate the presence of ink throughout the ventricular system of WT brains and in the rostral regions of mutant brains on both backgrounds. Representative images are shown. Scale bars represent 1 mm (lateral ventricle) and 125 μm (aqueduct of Sylvius and fourth ventricle).

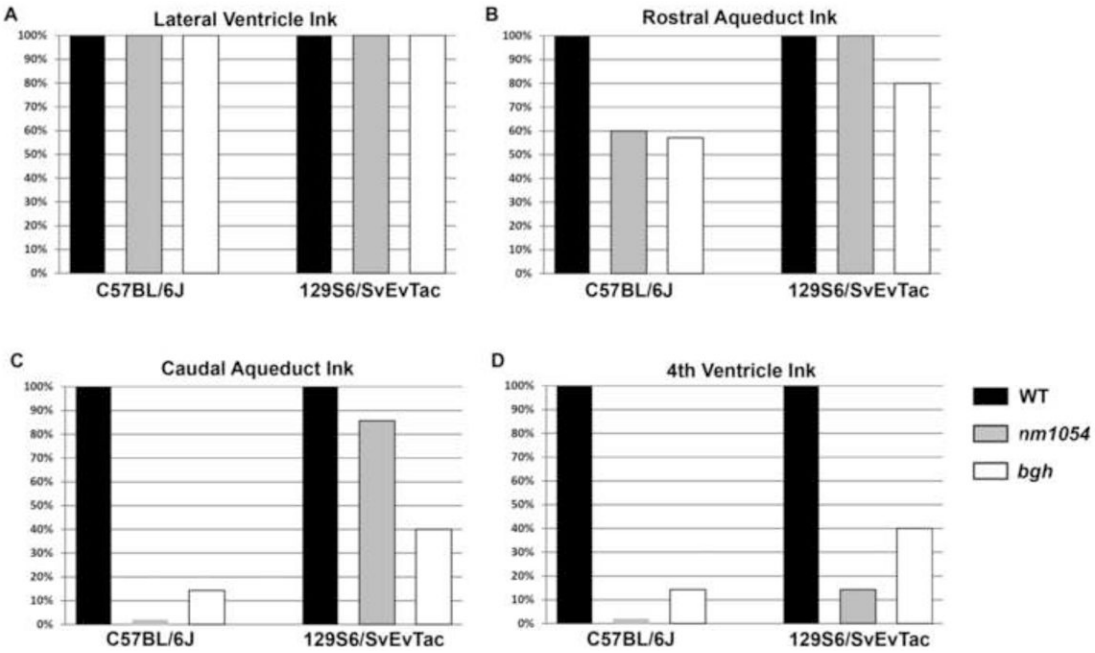

Figure 9. Frequency of ink in the ventricular systems of *nm1054* and *bgh* mutants after injection

Percentage of WT, *nm1054*, and *bgh* mice with India ink in the lateral ventricles (A), the rostral region of the aqueduct of Sylvius (B), the caudal region of the aqueduct of Sylvius (C), and the fourth ventricle (D) after injection into the lateral ventricles. The presence of ink decreases in both mutants in the caudal regions of the ventricular system, with a majority of mutants on both genetic backgrounds showing an absence of ink in the fourth ventricle.